J Nanopart Res (2009) 11:1339–1348
DOI 10.1007/s11051-009-9691-1

RESEARCH PAPER

Photocatalytic activity of nanostructured TiO_2 films produced by supersonic cluster beam deposition

Flavio Della Foglia · Tonia Losco · Paolo Piseri · Paolo Milani · Elena Selli

Received: 7 June 2008 / Accepted: 22 April 2009 / Published online: 7 July 2009

Abstract The photocatalytic activity of thin, nanostructured films of titanium dioxide, synthesized by supersonic cluster beam deposition (SCBD) from the gas phase, has been investigated employing the photodegradation of salicylic acid as test reaction. Because of the low deposition energy, the so-deposited highly porous TiO_2 films are composed of nanoparticles maintaining their original properties in the film, which can be fully controlled by tuning the deposition and post-deposition treatment conditions. A systematic investigation on the evolution of light absorption properties and photoactivity of the films in relation to their morphology, determined by AFM analysis, and phase composition, determined by Raman spectroscopy, has been performed. The absorption and photocatalytic activity of the nanostructured films in the visible region could be enhanced either through post-deposition annealing treatment in ammonia containing atmosphere or employing mild oxidation conditions, followed by annealing in N_2 at 600 °C.

F. Della Foglia · T. Losco · P. Piseri · P. Milani
Dipartimento di Fisica and C.I.MA.I.NA, Università degli Studi di Milano, Via Celoria 16, Milan 20133, Italy

E. Selli (✉)
Dipartimento di Chimica Fisica ed Elettrochimica and C.I.MA.I.NA, Università degli Studi di Milano, Via Golgi 19, Milan 20133, Italy
e-mail: elena.selli@unimi.it

Keywords Supersonic cluster beam deposition · Titanium dioxide films · Photocatalytic activity · Nanomaterials · Semiconductors

Introduction

Photocatalytic processes taking place on semiconductor surfaces have received particular attention during the past three decades, not only as environmentally friendly and low cost methods for water and air purification (Hoffmann et al. 1995; Zhang et al. 2000; Chen and Mao 2007), but also for the production of hydrogen by splitting of water (Fujishima and Honda 1972; Bolton 1996; Khaselev and Turner 1998; Grätzel 2001; Ni et al. 2007). Photocatalytic reactions on semiconductors are initiated by the excitation of the semiconductor with light of energy equal to or greater than its band gap. Consequently, an electron is promoted from the valence band (VB) to the conduction band (CB) and an electron (e^-_{CB}) hole (h^+_{VB}) pair is formed. These charge carriers can induce the reduction of electron acceptor species and the oxidation of electron donor species, respectively, adsorbed on the semiconductor surface.

The production of hydrogen and oxygen from photocatalytic water cleavage can take place under anaerated conditions, provided that electrons photopromoted in the CB are able to reduce protons, i.e.,

$E_{CB} < E°(H_2/H^+)$ on the electrochemical scale, and the holes photoproduced in the VB are able to oxidize water toward oxygen, i.e., $E_{VB} > E°(O_2/H_2O)$. On the other hand, oxidation of organic compounds takes place in the presence of oxygen (air) and mainly involves their direct or indirect (i.e., $^{\bullet}OH$ radical mediated) reaction with photogenerated holes, h^+_{VB}.

In consideration of its high activity, chemical inertness, low cost and non-toxicity, titanium dioxide is by far the most used and investigated photocatalyst (Fujishima et al. 2000; Ni et al. 2007). However, both its two most common polymorphs, i.e., anatase and rutile, possess photocatalytic properties mainly under UV radiation (Ni et al. 2007) and this makes the use of solar irradiation scarcely practicable in photocatalysis with unmodified TiO_2. For this reason, many efforts were concentrated toward the optical band gap narrowing of nanocrystalline titania (Anpo et al. 2002).

Amongst the different strategies proposed, doping with non-metallic impurities is regarded as superior to doping TiO_2 with transition metals (Cr, Fe, Ni, V), which leads to materials that suffer from thermal instability and increased number of carrier recombination centers (Choi et al. 1994). Since 2001, when Asahi et al. revealed that doping with nitrogen is effective in narrowing the band gap of TiO_2 and yield photocatalytic activity under visible light irradiation, there has been a continuously increasing interest in TiO_2 doping with anionic impurities such as carbon (Khan et al. 2002; Sakthivel and Kisch 2003; Nakano et al. 2005a, b), nitrogen (Irie et al. 2003; Sakthivel et al. 2004; Gole et al. 2004; Di Valentin et al. 2007), sulfur (Umebayashi et al. 2002), fluorine (Ho et al. 2006), and phosphorus (Yu et al. 2003). The observed band gap shift from the UV into the visible region has been attributed to substitution of lattice oxygen by the anions or formation of interstitial species, both giving rise to localized states in the band gap of the oxide. Because of its comparable atomic size with oxygen, small ionization energy, and stability (Qiu and Burda 2007), nitrogen doping appears as most practicable; a great variety of procedures, including physical treatments such as sputtering (Asahi et al. 2001; Nakano et al. 2005a, b) and implantation (Diwald et al. 2004), or chemical treatments (Asahi et al. 2001; Irie et al. 2003; Qiu and Burda 2007), sol-gel syntheses (Sakthivel et al. 2004; Gole et al. 2004; Lin et al. 2005), oxidation of titanium nitride (Morikawa et al. 2001; Chen and Burda 2008), have been used to incorporate nitrogen in titanium dioxide.

Besides light absorption properties, also the nanostructure of semiconducting materials profoundly affects their catalytic activity. Due to the magnification of surface effects, nanocrystalline semiconductors present radically different and generally improved photocatalytic properties compared to their bulk counterpart (Carotta et al. 1999). Large surface area and nanocrystalline structure, together with the specific properties of doped materials, allow to improve energy conversion rates and point to this kind of photocatalytic materials as important candidates for solar energy harvesting and storage in chemical form.

Here, we present the first characterization of the photocatalytic properties of cluster-assembled nanostructured TiO_2 films using, as a test, the degradation of salicylic acid (SA) under UV light irradiation, a reaction which can be easily monitored by fluorescence analysis in low reaction volumes (Macyk and Kisch 2001). Our nanostructured titanium dioxide films are produced by supersonic cluster beam deposition (SCBD) (Barborini et al. 2002, 2005) and possess high porosity. A systematic investigation of the evolution of their photoactivity after different deposition conditions or post deposition thermal treatment in controlled atmosphere has been performed, aiming at the optimization of cluster-assembled films for photocatalytic uses, with the final target of attaining efficient photoactivity under visible light.

Experimental

Film deposition and modification

TiO_2 films were deposited on rectangular (9.0×50.0 mm^2), 1 mm thick spectroscopic-grade quartz or silicon supports by the SCBD apparatus, equipped with a Pulsed Microplasma Cluster Source (PMCS), described in detail elsewhere (Barborini et al. 1999). In brief, a titanium target, inserted in the PMCS, is sputtered by a plasma confined in a jet of inert gas (He or Ar). Sputtered Ti atoms thermalize within the inert gas and condense to form clusters. The mixture of clusters and inert gas is then extracted from the PMCS in vacuum through a nozzle to form a seeded supersonic beam that is collected on a

substrate located in the beam trajectory. The cluster kinetic energy is low enough to avoid fragmentation, and hence a nanostructured film is grown. The mass distribution of the clusters can be controlled to tailor the nanostructure of the film (Kholmanov et al. 2003).

The as-deposited films have a porous structure with density of 2.5–2.7 g cm^{-3}, as obtained by optical methods (Barborini et al. 2005), and consist of nanocrystals with size below 10 nm embedded in an amorphous matrix, according to previous TEM and XRD analysis (Barborini et al. 2002, 2005). In the present study, ca. 100 nm thick films have been deposited, consisting of highly oxygen deficient under-stoichiometric TiO_x nanoparticles, as revealed by their initial dark, metallic color. The first oxidation of such materials, evidenced by their turning into transparent films, is achieved during their first exposition to air; grain size and crystal order can be refined by post deposition thermal treatment under different conditions. The granular structure of the as-deposited films can be appreciated in Fig. 1.

Post-deposition annealing was performed in this study under different gases or gas mixtures (air, N_2, Ar/NH_3, Ar/O_2) in an open joule furnace for 3 h at constant temperature (200–1000 °C, measured with a K-type thermocouple). When not otherwise specified, standard annealing conditions were adopted, consisting in 3-h long treatment in an Ar/O_2 80/20 mixture at 600 °C. Complete oxidation of the films can be attained after this treatment, as evidenced by their final transparency; visible light absorbing films appeared yellowish. Twin films were always deposited under identical SCBD conditions, either on quartz (for reflectance and photocatalytic characterization) or on silicon (for Raman and AFM characterization).

Structural characterization of the films

Cluster-assembled films were characterized by atomic force microscopy (AFM) using a Digital Instruments Multimode Nanoscope IV (Veeco) microscope operated in tapping mode with single-crystal silicon cantilever tip.

Raman spectra of the films deposited on silicon were recorded by a home assembled spectroscopic system consisting in an Ar ion laser emitting at 514 nm (Spectra Physics, beamlok series 2065-7) as excitation source, a single monochromator (Acton SP-2558-9N) equipped with a 1200 blaze mm^{-1} grating, a notch filter (Razoredge long wave pass filter), and a liquid nitrogen-cooled CCD camera (Roper-Princeton Instruments SPEC10:400B/LN). The evolution of the crystalline structure of the TiO_2 film could be monitored by the change of the Raman lines at 144 and 633 cm^{-1}, assigned to the modes of the anatase phase, and of the 447 and 612 cm^{-1} modes, typical of the rutile phase.

UV–Vis diffuse reflectance spectra of the TiO_2 films were measured with a Perkin-Elmer Lambda 35 apparatus equipped with an integration sphere (Labsphere RSA-PE-20). Reflectance spectra were recorded with our smooth and transparent films placed over a total white reference support.

Photocatalytic activity tests

The photocatalytic activity of the films was tested in the oxidative degradation of SA. Nanostructured TiO_2 films immersed in an aqueous solution of SA (initial concentration 1.0×10^{-4} M) were irradiated employing a medium pressure mercury arc lamp as irradiation source (Oriel), mounted on an optical bench. A 80 mm diameter lens was placed between the lamp and the irradiated cuvette holder, to collimate the photon flux and make it perpendicular to the cuvette wall. A cut-off filter at 320 nm was usually employed to limit direct SA photolysis. According to ferrioxalate actinometry (Hatchard and Parker 1956), the light intensity on the irradiated cuvette under such conditions was $(1.39 \pm 0.08) \times 10^{-5}$ Einstein s^{-1} dm^{-3}, and it decreased to $(5.2 \pm 0.4) \times 10^{-6}$ Einstein s^{-1} dm^{-3} when a 400 nm cut-filter was employed.

The irradiated quartz cuvette has two compartments, both initially filled with the SA solution. The TiO_2 film was placed in the second compartment, on the internal cuvette wall at the maximum distance from the lamp and facing it. Thus, the light first passed through the compartment containing only the SA solution, employed as a reference, and then entered the compartment containing also the TiO_2 film. The variation of SA concentration was determined by fluorimetric analysis, by means of a Perkin Elmer 650-10S fluorescence spectrometer, with 300 nm excitation wavelength and 420 nm emission wavelength. Both the irradiated cuvette and the cell holder in the fluorimeter were thermostated at 35 °C, to avoid any fluorescence fluctuation with temperature. Due to

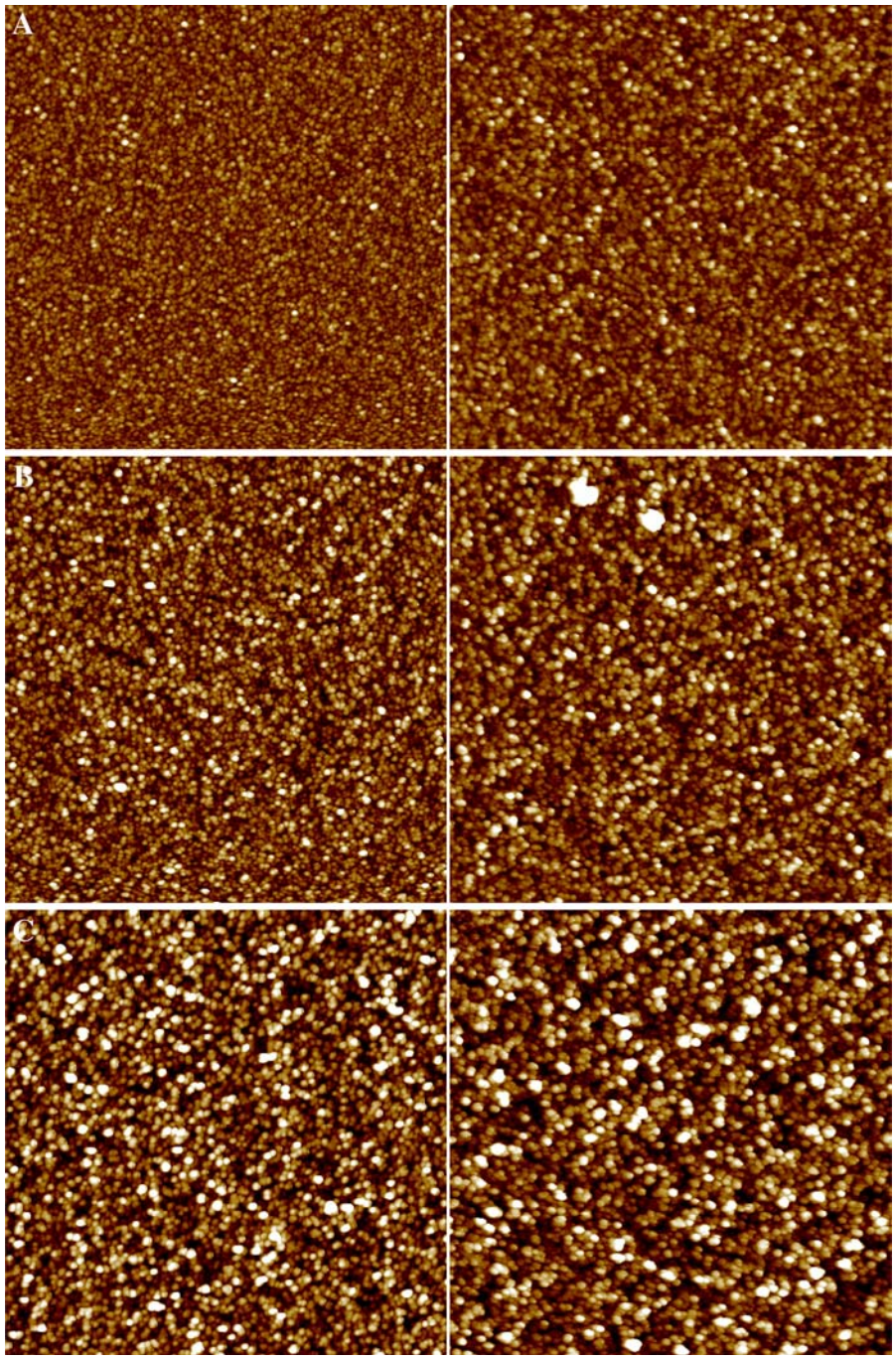

Fig. 1 AFM images of TiO_2 films of increasing thickness (from **a**–**c**) before (*left*) and after (*right*) annealing at 600 °C in an Ar/O_2 80/20 atmosphere. All image sizes are 2 μm × 2 μm. Thickness, roughness, and area data of the films, obtained by AFM analysis, are reported in Table 1

the low concentration of the solutions, SA concentration can be assumed proportional to the fluorescence intensity signal (Macyk and Kisch 2001), its degradation products being non-fluorescent at room temperature. Thus, the difference between the fluorescence signal of SA of the two solutions could be

directly related to the photocatalytic action of the TiO_2 film in contact with the second one.

Films deposited and thermally annealed under different conditions were irradiated for a fixed length of time. Significant direct SA photolysis (i.e., degradation in the front compartment solution) occurred under irradiation with the full lamp spectrum; however, it was always below 10% of the initial SA content, when the light was filtered through a 320 nm cut off filter. Blank runs performed with no photocatalyst film in the second compartment confirmed that SA photolysis proceeded up to the same extent in the two cell compartments. No direct SA photolysis was ever observed when employing the 385 and 400 nm filters. Percent photocatalytic SA degradation was calculated as $D(\%) = (1 - C/C_R) \times 100$, C and C_R being, respectively, the residual SA concentration in contact with the film and in the front cuvette compartment, after a certain irradiation time.

Results and discussion

The morphology of cluster-assembled TiO_2 films and its dependence on thickness and post-deposition treatments is shown in Fig. 1. All films have a uniform structure characterized by nanoparticles forming randomly assembled nanograins of slightly different dimensions (from 15 to 60 nm), increasing with increasing the film thickness. The characterization of the morphological features of the films performed by AFM is reported in Table 1. In general, their thickness, roughness, and area did not undergo great modification after the treatment; the films clearly remained nanostructured, though some grain growth occurred (Fig. 1). After annealing the thickness of the film decreased, the roughness of thinner films decreased, while the area slightly increased, demonstrating that annealing might improve not only the crystallinity (see below), but also the morphology of the nanostructured TiO_2 films for photocatalytic uses. In fact, an increase in the exposed surface area of the photocatalyst, where the substrates of photocatalytic reactions may adsorb and undergo photoinduced electron transfer processes, is expected to be beneficial in photocatalysis.

Figure 2 exhibits the Raman spectra of ca. 100 nm thick TiO_2 film annealed at 200, 400, 600, 800, and 1000 °C in an Ar/O_2 80/20 atmosphere. After annealing at 200 °C, no crystalline structure can be evidenced by Raman spectroscopy, i.e., the film is prevalently amorphous. After annealing at 400 °C, the lowest frequency mode of the anatase phase at 144 cm^{-1} becomes well resolved, indicating that the anatase phase formed below 400 °C. The other E_g anatase line at 639 cm^{-1} (Zhang et al. 2006) is also present in the spectrum after annealing at 400 °C, though its intensity is much lower. Both lines are marked by vertical arrows in Fig. 2. However, the intensity of the anatase modes becomes progressively lower with increasing the annealing temperature and practically disappears above 800 °C, while after annealing at 800 °C two peaks at 447 cm^{-1} and at 612 cm^{-1} (also marked by arrows in Fig. 2) become evident and even more intense after annealing at 1000 °C. These peaks correspond to the E_g and A_{1g} modes of the rutile phase, respectively (Zhang et al. 2006). This indicates that anatase is transformed into rutile at temperature above 600 °C and that rutile is the only phase above 800 °C.

Supersonic cluster beam deposition TiO_2 films absorb light at wavelengths shorter than 300 nm. As shown in Fig. 3, the reflectance spectra of films annealed under standard conditions (i.e., in Ar/O_2 80/20 mixture) at progressively higher temperature exhibit a progressive shift toward longer wavelengths. This reflects in part the progressively higher content of the rutile phase, characterized by a somewhat

Table 1 Structure parameters of SCBD films determined by AFM analysis before and after annealing under standard conditions (at 600 °C in a Ar/O_2 80/20 mixture)

Sample	Thickness as deposited (nm)	Thickness annealed (nm)	Roughness as deposited (nm)	Roughness annealed (nm)	Area as deposited	Area annealed
A	17.3 ± 1.6	14.5 ± 0.3	3.4 ± 0.1	3.0 ± 0.1	1.10 ± 0.01	1.15 ± 0.01
B	47.6 ± 4.4	35.2 ± 2.2	4.9 ± 0.1	4.7 ± 0.1	1.17 ± 0.01	1.24 ± 0.01
C	89.9 ± 5.0	84.5 ± 6.0	6.9 ± 0.1	6.9 ± 0.1	1.21 ± 0.01	1.30 ± 0.01

Area indicates the ratio between the surface area determined by AFM analysis and the corresponding flat geometrical area

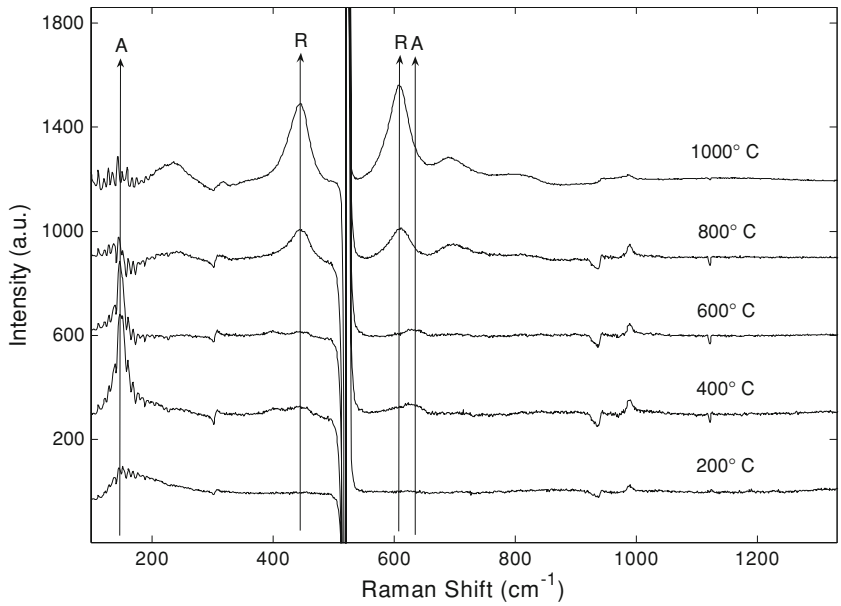

Fig. 2 Raman spectra of TiO_2 films (ca. 100 nm thick) annealed in Ar/O_2 80/20 at different temperature, showing the appearance of the anatase phase after annealing at 400 °C (144 and 639 cm^{-1} modes) and the progressive increase of the 447 and 612 cm^{-1} active modes of rutile after annealing above 600 °C

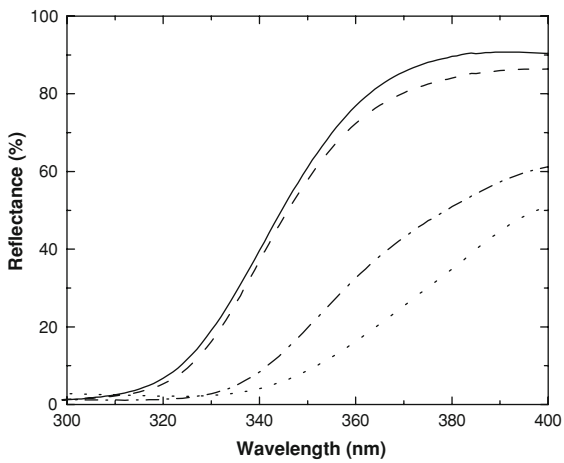

Fig. 3 UV–vis reflectance spectra (300–400 nm range) of TiO_2 films (ca. 100 nm thick) annealed in Ar/O_2 80/20 for 3 h at different temperature: (——) 400 °C; (**- - -**) 600 °C; (– · – · –) 800 °C; (· · · ·) 1000 °C

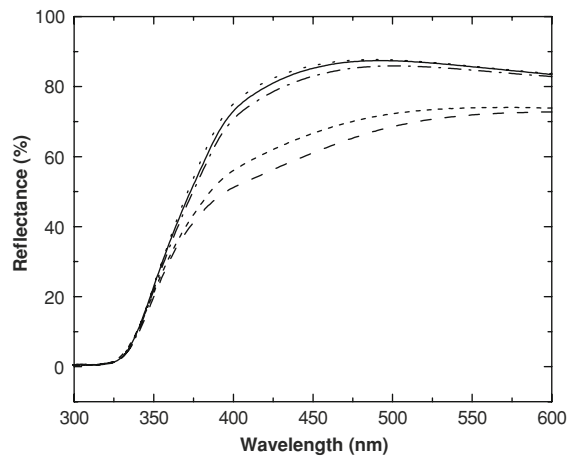

Fig. 4 UV–vis reflectance spectra of different films annealed at 600 °C for 3 h, if not otherwise specified, in different atmosphere: (- - -) Ar/NH_3 95/5; (· · · ·) Ar/NH_3 95/5, followed by Ar/O_2 80/20 at 500 °C for 2 h; (– · – · –) Ar/NH_3 95/5 atmosphere containing only O_2 traces; (——) Ar/O_2 80/20 (standard conditions); (– – – – –) Ar/O_2 80/20 a 200 °C for 1 h, followed by pure N_2 at 600 °C for 3 h

narrower bandgap (i.e., around 3.2 eV) with respect to anatase, and the increase of the grain size after annealing at high temperature (Barborini et al. 2005), increasing the extent of light scattering. Films annealed in the presence of different gases or gas mixtures, and particularly those annealed in the presence of ammonia or oxidized under mild conditions, exhibit different reflectance features, with light absorption ability extending into the visible region. Such reflectance spectra, shown in Fig. 4, will be discussed in more detail later on, in relation with structural and doping effects on their photocatalytic activity.

Because of the small dimensions of the TiO_2 films deposited on quartz specimens, which are compatible with their possible exploitation in the fabrication of microdevices, we investigated their photocatalytic activity in an oxidative photodegradation test

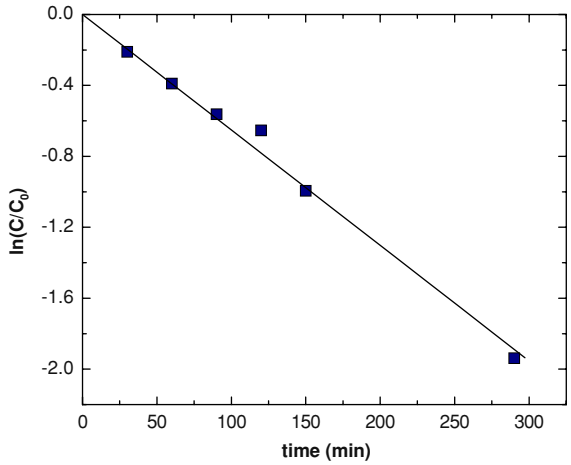

Fig. 5 Decrease of SA concentration with irradiation time, in the form of first order rate plot, observed under irradiation with a 320 cut off filter of a SA solution (initial concentration $C_0 = 1.0 \times 10^{-4}$ M) in contact with a ca. 200 nm thick TiO_2 film, annealed under standard conditions

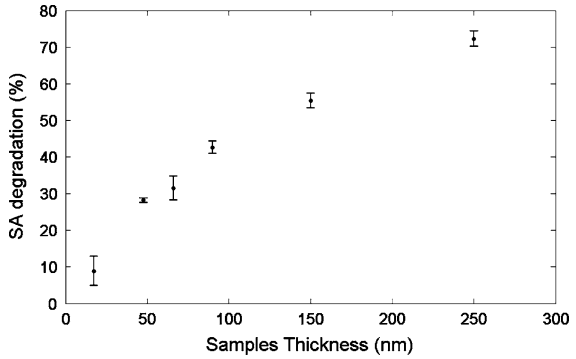

Fig. 6 Percent SA degradation as a function of the TiO_2 film thickness after 160 min photocatalytic irradiation with the 320 nm cut off filter in the presence TiO_2 films annealed under standard conditions

reaction, which could be easily investigated in small reaction volumes (<2 cm^3 in our case). The photocatalytic degradation of SA fulfills these requirements, due to the fluorescence properties of SA undergoing photocatalytic degradation by $^{\bullet}OH$ radical attack and/or direct oxidation by VB holes (Macyk and Kisch 2001).

Cluster-assembled TiO_2 films definitely exhibit photocatalytic activity under 320 nm-filtered excitation. Kinetic analysis of the residual fluorescence intensity at different irradiation time indicates that SA degradation occurs according to a first order rate law, which is quite typical in photocatalysis (Ollis 2005). Figure 5 shows an example of kinetic data obtained with a standard film and reported according to the integrated first order rate law. From the rate constant obtained from these data, equal to $(6.58 \pm 0.08) \times 10^{-3}$ min^{-1}, and the irradiation intensity under the adopted experimental conditions, determined by ferrioxalate actinometry, an apparent photon efficiency of 0.08% is obtained.

The photocatalytic activity of the SCBD films was found to depend on both deposition parameters and post-treatment conditions. A first series of measurements was devoted to investigate the effects of the film thickness in specimens annealed under standard conditions. The percent SA degradation attained after 160 min irradiation is reported in Fig. 6 as a function of the film thickness, evaluated by AFM analysis. The photocatalytic activity clearly increased with increasing the film thickness (and the amount of photocatalyst), though with a progressively lower slope, i.e., according to a typical saturation behavior. With increasing the amount of TiO_2 nanoparticles in contact with the SA-containing aqueous phase, interface electron transfer processes on the excited semiconductor occur at a higher rate, and the rate of SA degradation consequently increases. However, this takes place as long as the semiconductor nanoparticles are fully excited by light, non-irradiated TiO_2 particles in internal layers being inactive. The observed saturation behavior with increasing film thickness eventually tends to a photocatalytic activity plateau, falling outside the film thickness range examined in this work (i.e., for thickness values above 300 nm), corresponding to maximum light absorption by the exposed film surface.

Then the effects on the photocatalytic activity of the gas employed in post-deposition treatments at different temperature were investigated systematically. As shown in Fig. 7, the type of gas (air, methane, Ar) first contacted with the as-deposited film was found to influence the photocatalytic properties of the films after annealing in air. In fact, the films first contacted with argon and then annealed in air at different temperature exhibit a lower photocatalytic performance with respect to those first contacted with air or methane and then annealed in air. On the other hand, the photocatalytic activity of the films exhibits a remarkable dependence on the annealing temperature, with a common trend for all specimens, almost independent of the first contact gas

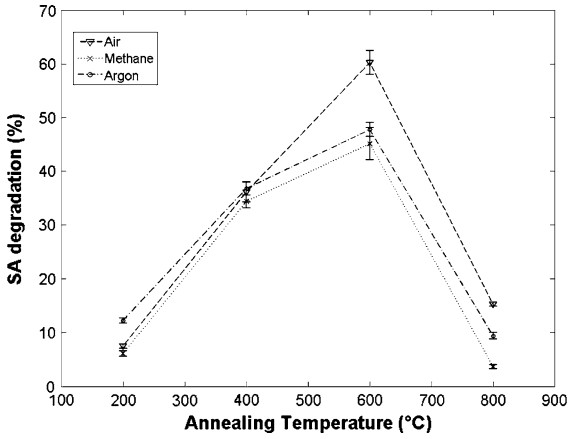

Fig. 7 Percent SA degradation after 3 h irradiation ($\lambda_{irr} > 320$ nm) as a function of the annealing temperature of the SCBD film in air and of the type of first contact gas after deposition

(Fig. 7). It is worth recalling that the annealing temperature determines both the particle dimensions and, consequently, the morphology of the film, and its structural properties, in particular its crystalline phase composition. The photocatalytic activity of the films annealed below 200 °C is very low, because they are not sufficiently crystalline (Kholmanov et al. 2003). The highest photocatalytic activity was attained with a film first contacted with air and then annealed in air at 600 °C, but high activities were shown also by films first contacted with methane and argon and then annealed in air at the same temperature (Fig. 7). Under standard conditions, 600 °C appears to be the optimal annealing temperature. The film contains both the anatase and the rutile phase and their coexistence may have extremely positive effects on photocatalysis, by favoring photoproduced charges separation (Ohno et al. 2001).

Annealing under different controlled atmosphere was finally explored as a means to modify the crystalline structure of the films, by influencing their nanostructure and reducing the bandgap through the introduction of structural or substitutional defects (Asahi et al. 2001), with the final aim of imparting absorption properties together with photocatalytic activity in the visible. Identical, ca. 200 nm-thick SCBD films were first contacted with air and then underwent different 3-h long post deposition treatments, usually at 600 °C. The highly porous and defective structure of the as-deposited films would be ideal to allow efficient incorporation of dopant species and/or oxygen defects during post-deposition annealing under different conditions.

As shown in Fig. 4, the films annealed under standard conditions (Ar/O_2 80/20 mixture) showed the typical absorption onset at ca. 420 nm. An average 44% photocatalytic SA degradation, $D(\%)$, was attained with these films after 2-h long irradiation with $\lambda_{irr} > 320$ nm, which decreased to 2.5% and below 0.5% for $\lambda_{irr} > 385$ nm and $\lambda_{irr} > 400$ nm, respectively.

Annealing in an Ar/NH_3 95/5 atmosphere lead to a TiO_2 film with a markedly increased absorption in the visible region (long dashed line in Fig. 4). However, this did not correspond to an improvement in photocatalytic activity: a $D(\%)$ value of only 21% was attained under 2-h long irradiation through the 320 nm cut off filter and $D(\%)$ dropped below 0.7% under longer wavelengths irradiation. The photocatalytic activity of this specimen decreased after storage in air for several months. Thus, a very small activity in the visible, possibly originated by light absorption also from the inter bandgap energy states introduced by nitrogen doping, was accompanied by a lower performance under UV irradiation. This can be ascribed to the persistence of Ti metal clusters or, at least, extended oxygen defects in an insufficiently oxidative atmosphere (Irie et al. 2003), which would act as scavengers of photoproduced charge carriers.

Aiming at attaining a more extended oxidation of the SCBD layer during annealing, another film was first treated with Ar/NH_3 (95/5) for 3 h at 600 °C and then in Ar/O_2 (80/20) for 2 h at 500 °C. After this treatment, its reflectance spectrum was very similar to that of the film directly annealed under standard conditions (Fig. 4). This indicates that nitrogen doping is reversible at relatively high temperature and that the standard properties of the film are totally recovered by oxygen treatment. This hypothesis is confirmed by the fact that the photocatalytic activity of this film with $\lambda_{irr} > 320$ nm was almost identical to that of the film directly annealed under standard conditions, while it maintained a slightly improved activity under visible light irradiation (1.6% SA degradation after 2 h with $\lambda_{irr} > 400$ nm).

In order to favor oxidation during the thermal treatment in the presence of the rather reductive NH_3 gas, another film was treated in an Ar/NH_3 95/5 atmosphere containing O_2 traces (below 0.5%).

This film exhibited optical properties very similar to those of the standard sample, with only a minor absorption increase in the visible region (Fig. 4). The photocatalytic SA degradation on this film was 47%, 3.15%, and 0.95% after 2-h long irradiation through the 320, 385, and 400 nm cut off filter, respectively, i.e., slightly improved with respect to that obtained with the standard sample. The photocatalytic activity of this film did not change after storage in air for several months, in line with the hypothesis that the presence of small amounts of oxygen during the heat treatment at 600 °C in the presence of 5% ammonia limits the extent of oxygen defects within the oxide structure and leads to a stable and active N-doped TiO_2 film.

Finally, a SCBD film was annealed under controlled oxidizing conditions in the absence of ammonia, to ascertain the possibility of imparting visible light photoactivity also without N doping. After treatment in an Ar/O_2 80/20 mixture for 1 h at 200 °C and in pure N_2 for 3 h at 600 °C, the film exhibited a longer wavelength absorption onset (short dashed line in Fig. 4) and an average D(%) value of 47% with $\lambda_{irr} > 320$ nm and 2.7% with $\lambda_{irr} > 400$ nm after 2 h. Also in this case, the photoactivity remained unchanged for months. This demonstrates that annealing in the presence of NH_3 is not strictly necessary to improve visible light absorption and photoactivity of SCBD TiO_2 films, which could be attained also through the introduction of structure defects.

Conclusions

TiO_2 films produced by SCBD showed photocatalytically active in SA photodegration. Their activity depends on their morphology and stoichiometry at the nanoscale and can be modified by varying cluster production and deposition conditions and by post-deposition thermal annealing under different atmospheres. Post-deposition annealing in the presence of ammonia is able to introduce stable photoactivity in the visible without reducing activity in the UV-region, only if sufficiently oxidative conditions are ensured during the annealing process.

The demonstration that photocatalytic layers can be produced by SCBD is important in view of the integration of photocatalytic materials on microfabricated devices and reactors by exploiting the very high lateral resolution and compatibility with microfabrication processes typical of SCBD.

Acknowledgment This work was supported by CARIPLO Foundation, through the project entitled "Development of nanostructured photocatalytic films for energy conversion on microplatforms."

References

Anpo M, Takeuchi M, Ikeue K, Dohshi S (2002) Design and development of titanium oxide photocatalysts operating under visible and UV light irradiation. The applications of metal ion-implantation techniques to semiconducting TiO_2 and Ti-zeolite catalysts. Curr Opin Solid State Mater Sci 6:381–388. doi:10.1016/S1359-0286(02)00107-9

Asahi R, Morikawa T, Ohwaki T, Aoki A, Taga Y (2001) Visible-light photocatalysis in nitrogen-doped titanium oxide. Science 293:269–271. doi:10.1126/science.1061051

Barborini E, Piseri P, Milani P (1999) A pulsed microplasma source of high intensity supersonic carbon cluster beam. J Phys D 32:L105–L109. doi:10.1088/0022-3727/32/21/102

Barborini E, Kholmanov IN, Piseri P, Ducati C, Bottani CE, Milani P (2002) Engineering the nanocrystalline structure of TiO_2 films by aerodynamically filtered cluster deposition. Appl Phys Lett 81:3052–3054. doi:10.1063/1.1510579

Barborini E, Conti AM, Kholmanov I, Piseri P, Podestà A, Milani P, Cepek C, Sakho O, Macovez R, Sancrotti M (2005) Nanostructured TiO_2 films with 2 eV optical gaps. Adv Mater 17:1842–1846. doi:10.1002/adma.200401169

Bolton JR (1996) Solar photoproduction of hydrogen: a review. Sol Energy 57:37–50. doi:10.1016/0038-092X(96)00032-1

Carotta MC, Ferroni M, Guidi V, Martinelli G (1999) Preparation and characterization of nanostructured titania thick films. Adv Mater 11:943–946. doi:10.1002/(SICI)1521-4095(199908)11:11<943::AID-ADMA943>3.0.CO;2-L

Chen X, Burda C (2008) The electronic origin and the visible-light absorption properties of C-, N- and S-doped TiO_2 materials. J Am Chem Soc 130:5018–5019. doi:10.1021/ja711023z

Chen X, Mao SS (2007) Titanium dioxide nanomaterials: synthesis, properties, modifications, and applications. Chem Rev 107:2891–2959. doi:10.1021/cr0500535

Choi W, Termin A, Hoffmann MR (1994) The role of metal ion dopants in quantum-sized TiO_2: correlation between photoreactivity and charge carrier recombination dynamics. J Phys Chem 98:13669–13679. doi:10.1021/j100102a038

Di Valentin C, Finazzi E, Pacchioni G, Selloni A, Livraghi S, Paganini MC, Giamello E (2007) N-doped TiO_2: theory and experiment. Chem Phys 339:44–56. doi:10.1016/j.chemphys.2007.07.020

Diwald O, Thompson TL, Goralski EG, Walck SD, Yates JT Jr (2004) The effect of nitrogen ion implantation on the photoactivity of TiO_2 rutile single crystal. J Phys Chem B 108:52–57. doi:10.1021/jp030529t

Fujishima A, Honda K (1972) Electrochemical photolysis of water at a semiconductor electrode. Nature 238:37–38. doi:10.1038/238037a0

Fujishima A, Rao TN, Tryk DA (2000) Titanium dioxide photocatalysis. J Photochem Photobiol C 1:1–21. doi:10.1016/S1389-5567(00)00002-2

Gole JL, Stout JD, Burda C, Lou Y, Chen X (2004) Highly efficient formation of visible light tunable $TiO_{2-x}N_x$ photocatalysts and their transformation at the nanoscale. J Phys Chem B 108:1230–1240. doi:10.1021/jp030843n

Grätzel M (2001) Photoelectrochemical cells. Nature 414:338–344. doi:10.1038/35104607

Hatchard CG, Parker CA (1956) A new sensitive chemical actinometer II. Potassium ferrioxalate as a standard chemical actinometer. Proc R Soc Lond A Math Phys Sci 235:518–536. doi:10.1098/rspa.1956.0102

Ho W, Yu JC, Lee S (2006) Synthesis of hierarchical nanoporous F-doped TiO_2 spheres with visible light photocatalytic activity. Chem Commun (Camb) (10):1115–1117. doi:10.1039/b515513d

Hoffmann MR, Martin ST, Choi W, Bahnemann DW (1995) Environmental applications of semiconductor photocatalysis. Chem Rev 95:69–96. doi:10.1021/cr00033a004

Irie H, Watanabe Y, Hashimoto K (2003) Nitrogen concentration dependence on photocatalytic activity of $TiO_{2-x}N_x$ powders. J Phys Chem B 107:5483–5486. doi:10.1021/jp030133h

Khan SUM, Al-Shanhry M, Ingler WB Jr (2002) Efficient chemical water splitting by chemically modified n-TiO_2. Science 297:2243–2245. doi:10.1126/science.1075035

Khaselev O, Turner JA (1998) A monolithic photovoltaic-photoelectrochemical device for hydrogen production via water splitting. Science 280:425–427. doi:10.1126/science.280.5362.425

Kholmanov IN, Barborini E, Vinati S, Piseri P, Podestà A, Ducati C, Lenardi C, Milani P (2003) The influence of the precursor clusters on the structural and morphological evolution of nanostructured TiO_2 under thermal annealing. Nanotechnology 14:1168–1173. doi:10.1088/0957-4484/14/11/002

Lin Z, Orlov A, Lambert RM, Payne MC (2005) New insights into the origin of visible light photocatalytic activity of nitrogen-doped and oxygen-deficient anatase TiO_2. J Phys Chem B 109:20948–20952. doi:10.1021/jp053547e

Macyk W, Kisch H (2001) Photosensitization of crystalline and amorphous titanium dioxide by platinum(IV) chloride surface complexes. Chem Eur J 7:1862–1867. doi:10.1002/1521-3765(20010504)7:9<1862::AID-CHEM1862>3.0.CO;2-G

Morikawa T, Asahi R, Ohwaki T, Aoki K, Taga Y (2001) Band gap narrowing of titanium dioxide by nitrogen doping. Jpn J Appl Phys 40:L561–L563. doi:10.1143/JJAP.40.L561

Nakano Y, Morikawa T, Ohwaki T, Taga Y (2005a) Electrical characterization of band gap states in C-doped TiO_2 films. Appl Phys Lett 87:052111/1–052111/3

Nakano Y, Morikawa T, Ohwaki T, Taga Y (2005b) Deep-level optical spectroscopy investigation of N-doped TiO_2 films. Appl Phys Lett 86:132104/1–132104/3

Ni M, Leung MKH, Leung DYC, Sumathy K (2007) A review and recent developments in photocatalytic water-splitting using TiO_2 for hydrogen production. Renew Sustain Energy Rev 11:401–425. doi:10.1016/j.rser.2005.01.009

Ohno T, Sarukawa K, Tokieda K, Matsumura M (2001) Morphology of a TiO_2 photocatalyst (Degussa, P-25) consisting of anatase and rutile crystalline phases. J Catal 203:82–86. doi:10.1006/jcat.2001.3316f

Ollis DF (2005) Kinetics of liquid phase photocatalyzed reactions: an illuminating approach. J Phys Chem B 109:2439–2444. doi:10.1021/jp040236f

Qiu X, Burda C (2007) Chemically synthesized nitrogen-doped metal oxide nanoparticles. Chem Phys 339:1–10. doi:10.1016/j.chemphys.2007.06.039

Sakthivel S, Kisch H (2003) Daylight photocatalysis by carbon modified titanium dioxide. Angew Chem Int Ed 42:4908–4911. doi:10.1002/anie.200351577

Sakthivel S, Janczarek M, Kisch H (2004) Visible light activity and photoelectrochemical properties of nitrogen-doped TiO_2. J Phys Chem B 108:19384–19387. doi:10.1021/jp046857q

Umebayashi T, Yamaki T, Itoh H, Asai K (2002) Band gap narrowing of titanium dioxide by sulfur doping. Appl Phys Lett 81:454–456. doi:10.1063/1.1493647

Yu JC, Zhang L, Zheng Z, Zhao J (2003) Synthesis and characterization of phosphated mesoporous titanium dioxide with high photocatalytic activity. Chem Mater 15:2280–2286. doi:10.1021/cm0340781

Zhang L, Macyk W, Lange C, Maier WF, Antonius C, Meissner D, Kisch H (2000) Visible-light detoxification and charge generation by transition metal chloride modified titania. Chem Eur J 6:379–384. doi:10.1002/(SICI)1521-3765(20000117)6:2<379::AID-CHEM379>3.0.CO;2-Z

Zhang J, Li M, Feng Z, Chen J, Li C (2006) UV Raman spectroscopic study on TiO_2 I. Phase transformation at the surface and in the bulk. J Phys Chem B 110:927–935. doi:10.1021/jp0552473